

Investigation of phosphorous doping effects on polymeric carbon dots: Fluorescence, photostability, and environmental impact



Bo Zhi^a, Miranda J. Gallagher^b, Benjamin P. Frank^b, Taeyjuana Y. Lyons^c, Tian A. Qiu^a, Joseph Da^b, Arielle C. Mensch^d, Robert J. Hamers^d, Zeev Rosenzweig^c, D. Howard Fairbrother^b, Christy L. Haynes^{a,*}

^a Department of Chemistry, University of Minnesota - Twin cities, Minneapolis, MN 55455, USA

^b Department of Chemistry, The Johns Hopkins University, Baltimore, MD 21218, USA

^c Department of Chemistry and Biochemistry, University of Maryland Baltimore County, Baltimore, MD 21250, USA

^d Department of Chemistry, University of Wisconsin, Madison, WI 53706, USA

ARTICLE INFO

Article history:

Received 9 October 2017

Received in revised form

30 November 2017

Accepted 2 December 2017

Available online 5 December 2017

ABSTRACT

Carbon dots have arisen as a potential alternative to traditional quantum dots since they fluoresce but are synthesized from sustainably sourced green chemicals. Herein, fluorescent nitrogen-doped polymeric carbon dots (CDs) were synthesized by using citric acid (CA) or malic acid (MA) as carbon precursors and ethylenediamine as the nitrogen precursor. Additionally, phosphoric acid was used as a doping agent for each type of CDs to evaluate the impact of incorporating phosphorus into the nanoparticles. Thus, four kinds of doped CDs (N-doped or N, P co-doped) were obtained and named as CACDs, CA-P-CDs, MACDs, and MA-P-CDs. Quantum yield and fluorescence lifetime analysis indicate that phosphorus doping of up to *c.a.* 10 wt% does not induce a remarkable influence on CD photoluminescence. The photostability of the N, P co-doped MACDs (MA-P-CDs), however, was observed to increase compared to the N-doped MACDs under 350 nm UV (UV-B) exposure. Lastly, to assess the impact of this emerging nanoparticle on prokaryotes, the bacterial toxicity of these CDs was tested using *Shewanella oneidensis* MR-1 as a model microorganism. Interestingly, the CDs exhibited no toxicity in most cases, and in fact facilitated bacteria growth. Hence, this work suggests that CDs are potentially eco-friendly fluorescent materials.

© 2017 Elsevier Ltd. All rights reserved.

1. Introduction

Since the discovery of carbon dots (CDs) during the purification of arc-discharged single-walled carbon nanotubes (SWCNTs) in 2004 [1], they have become a carbon nanoallotrope of great interest [2,3]. Generally, CDs are zero-dimensional (0D) carbon nanoparticles of 2–10 nm diameter with quasi-spherical morphology. The majority of the carbon within the CDs is sp³-hybridized and usually exists as amorphous carbon, different from another 0D carbon nanoallotrope, nanodiamonds (NDs), which consist of highly crystalline domains [2–5]. Due to their excellent photoluminescence, stability, low cost, and easy preparation [4,6–8], CDs have been under intense investigation for their potential applications in sensing [9–14], bioimaging or cell labelling [3,15–17], drug

delivery [16,17], white light-emitting devices [7,18], and energy conversion [19–21].

A variety of methods have been developed to generate fluorescent CDs in the past decade. Roughly, these synthesis approaches can be classified as either “top-down” or “bottom-up” [4,22]. Generally, the “top-down” route involves breaking down bulk carbon sources, like graphite [19,23], carbon fibers [24,25], or carbon nanotubes [1,26], into tiny carbon nanoparticles, namely, carbon dots. Available “top-down” synthetic techniques exploit electrochemistry, arc discharge, laser ablation, or plasma treatment [27,28]. Conversely, the “bottom-up” route refers to the construction of amorphous carbon nanostructures from molecular precursors such as saccharides [29], organic acids [8,13], or amino acids [30,31] via combustion methods, hydrothermal/solvothermal treatment, or microwave irradiation [4,27]. To be more specific, microwave heating-based synthesis capitalizes on internal precursor molecular rotation transitions coupling with external electromagnetic irradiation [32]. Thus, the heating efficiency is not

* Corresponding author.

E-mail address: chaynes@umn.edu (C.L. Haynes).

related to the thermal conductivity of the precursors, realizing an immediate on/off switching in heating [32,33]. Hence, compared to other methods, microwave-assisted thermal treatment conserves both time and energy, and might even avoid undesirable side reactions or facilitate new reaction routes [32–34]. Thus, microwave heating has been broadly used as a promising method to prepare stable and highly photoluminescent CDs [7,8,35–39].

Doping heteroatoms into CDs has been a popular concept for potentially improving the performance of carbon nanomaterials [40–42]. A significant number of doped CD studies have been reported, most of them doped with non metal heteroatoms such as N [43–45], S [44,46], B [47–49], or P [49–51]; there are also rare cases of metal atom dopants such as Cu [52], Mg [53] and Gd [54]. In general, doped CDs have exhibited improved optical properties compared to non-doped CDs such as higher quantum yields and longer fluorescence lifetimes, especially when a functionalization route is used. The chemical identity of the doped heteroatom influences the electron distribution within the CDs, altering the band-gap energy and thus improving the CD photoluminescence [55,56]. Currently, there are a lack of systematic investigations on the effects of doping on the properties of CDs. To address this issue, a series of polymeric CDs with different levels of doping were synthesized herein to compare the fluorescence properties of these polymeric CDs, and to elucidate whether doping is an effective strategy for polymeric CD performance improvement. It is important to mention here that there is a range of names used for carbon dot nanomaterials, including carbon quantum dots, graphene quantum dots, and polymer dots. To avoid confusion, the products made in this work will be identified as polymeric CDs because they are generated by carbonizing polymerized intermediates.

CDs have exhibited comparable quantum yields to traditional semiconductor quantum dots (QDs), and they are free of toxic heavy metal ions [2,4]. Thus, they are assumed to be of low toxicity and may serve as a green alternative to QDs [57–59]. Up to now, most CD research has been heavily focused on their synthesis and applications, while only a few reports have addressed their potential environmental consequences, let alone the comparative impact of modified/doped CDs [60,61]. To evaluate their true potential, it is necessary to characterize CD photoluminescence in parallel with a toxicity assessment relevant to the potential release of CDs into the ecosystem – a specific goal of this study. Microorganisms, located at the bottom of the food web, are ubiquitous [62] and thus likely to first interact with and respond to nanomaterials released into the environment. *Shewanella oneidensis* MR-1 (*S. oneidensis* MR-1), first discovered in Lake Oneida, NY [63], is a species of Gram-negative bacteria important in the ecosystem based on its notable ability to reduce metal oxides via dissimilatory reduction under anaerobic conditions [64]. In addition, *S. oneidensis* MR-1 has been applied in nanomaterial toxicity screening, including studies of silver nanoparticles (Ag NPs) [65], gold nanoparticles (Au NPs) [66], and Li-ion battery materials [67]. Thus, *S. oneidensis* MR-1 has been chosen herein as the model microorganism to evaluate the potential environmental impact of N- and P-doped polymeric CDs.

In this manuscript, we will demonstrate the synthesis, material characterization, photostability tests, and bacterial toxicity of nitrogen and phosphorous-doped polymeric carbon dots. This is the first effort in a larger set of experiments, and future work will further explore the underlying chemical or physical properties of the polymeric carbon dots that result in the exciting photoluminescent properties.

Specifically, this work explores the impact of phosphorous doping on nitrogen-doped polymeric CDs. Based on quantitative analysis, we find that doping phosphorus into the polymeric CD structure using a phosphorous-containing precursor does not

significantly impact polymeric CD fluorescence behavior including quantum yield and lifetime. The phosphorus-doped polymeric CDs, however, do demonstrate enhanced photostability during UV-B exposure (350 nm) compared to undoped polymeric CDs. Interestingly, comparing the photoluminescence performance of nitrogen-doped polymeric CDs generated from citric acid, containing three carboxylic acid groups, versus the two carboxylic acid groups in malic acid, shows significant differences, likely due to their different crosslinking patterns with ethylenediamine. Furthermore, the bacterial toxicity results indicate that phosphorous doping did not increase toxic effects towards the bacteria but potentially stimulated bacteria growth in most cases, highlighting the potential of polymeric CDs as an emerging fluorescent nanomaterial with minimal adverse environmental effects.

2. Experimental

2.1. Chemicals

Citric acid (CA, ACS reagent, 99.5%), DL-malic acid (MA, ReagentPlus®, 99%), phosphoric acid (ACS reagent, 85% H₃PO₄) and ethylenediamine (ReagentPlus®, 99%) were purchased from Sigma Aldrich. Quinine sulfate dihydrate (99+%, ACROS Organics™) was obtained from Fisher Scientific. The Biotech cellulose ester (CE) membrane (MWCO 100–500 D) was obtained from Spectrum Labs. Deionized water was produced by a Millipore Milli-Q system (Billerica, MA), and used through all experiments. All other reagents were of analytical grade and used without further purification. Difco™ LB broth (Miller) and Difco™ agar (granulated) were purchased from Becton, Dickinson, and Company. Dulbecco's phosphate-buffered saline (DPBS) was purchased from Mediatech, Inc. Sodium chloride (NaCl) and 4-(2-hydroxyethyl)-1-piperazineethanesulfonic acid (HEPES) were purchased from Sigma Aldrich.

2.2. Synthesis of amorphous polymeric carbon dots

The synthesis was adopted from previous reports [8] with minor modifications. To synthesize the CACDs, a 4 M aqueous citric acid stock solution was prepared in advance. 2 mL of this stock solution was transferred into a 100-mL beaker, and then 540 μL of ethylenediamine was added. The reaction was completed within 1 min as heat was released and a homogenous solution was formed. The mixture was stirred for 30 min and allowed to cool. Then, the colorless transparent mixture was transferred to a domestic microwave oven and heated under 360 W for 3 min. The resultant orange-yellow foamy solid was cooled in a fume hood for 20 min before 10 mL of MQ water was added into the beaker. The obtained reddish-brown transparent solution was dialyzed for 24 h to remove unreacted precursors. Then, rotary evaporation was used to remove most of the water in the solution, leaving behind a brown solid product at the bottom. Further drying was completed in an oven at 40 °C for one day.

To generate varied phosphorus-doped citric acid polymeric carbon dots (the CA-P-CD series), 2 mL of citric acid stock solution was poured into a beaker, and then 34 μL of phosphoric acid was added. After mixing for 10 min, 540 μL ethylenediamine was added. The subsequent procedure was the same as followed for the CACDs. Thus, CA-P-CDs-1 were obtained. To synthesize CA-P-CDs-2, 3 and 4, phosphoric acid was added in quantities of 68, 136 and 272 μL, respectively. The final products of the CACDs and CA-P-CDs series were all yellow powders with gradually darker yellow color with increasing amount of doped phosphorus (Fig. S1A).

For the synthesis of MACDs and the MA-P-CD series (phosphorus-doped malic acid polymeric carbon dots), malic acid was

used as a carbon source instead of citric acid. The synthesis procedure was otherwise the same. All the final products in this series appeared as dark brown powders (Fig. S1B).

2.3. Material characterization

Extensive characterization was performed to learn as much about the chemical and structural characteristics of the CDs as possible. UV–vis extinction spectra were obtained using a Mikro-pack DH-2000 UV–Vis–NIR spectrometer. Fluorescence spectra were measured with a PTI QuantaMaster™ 400. Excitation emission matrices (EEMs) were collected on a Thermo Scientific Lumina fluorescence spectrometer (Waltham, MA, USA) with the 3D Scan Module using a 1 cm path length cell, 2.5 nm slit width, and internal correction for the lifetime of the photomultiplier tube with excitation from 200 to 600 nm (5 nm step size) and resultant emission collected from 300 to 750 nm (1 nm step size). Inner filter effects were avoided by using a dilute polymeric CD solution with an absorbance of 0.1 at the peak absorbance (*c.a.* 350 nm). The morphology and size distribution of polymeric CDs were examined using a FEI Tecnai G² F30 transmission electron microscopy (TEM) at 300 kV. The TEM samples were prepared by dropping an aqueous suspension of polymeric CDs onto a 300-mesh gold grid coated with an ultra-thin lacey carbon film. Wide-angle X-ray diffraction (XRD) data were collected by a Bruker-AXS (Siemens) D5005 XRD using Cu K α as the radiation source ($\lambda = 0.15418$ nm), with a step of 0.02 in the range from 10 to 70. The attenuated total reflection-Fourier transform infrared spectroscopy (ATR-FTIR) spectra were recorded with a Nicolet Magna-IR 750 spectrometer. The X-ray photoelectron spectroscopy (XPS) spectra were analyzed by a Surface Science SSX-100 using a monochromatic Al K α X-ray source (50 eV pass energy, and 0.9 eV energy resolution by the full width at half maximum of Au 4f_{7/2} peak) and a PHI 5600 XPS (58.7 eV pass energy, 0.125 eV/step, Mg K α X-rays) and processed with CasaXPS software (Teignmouth, UK). Energy dispersive X-ray (EDAX) was performed on a JEOL 6700F SEM using a 20-kV electron beam using an EDAX Genesis 4000 X-ray analysis system as a detector. Atomic force microscopy (AFM) images were collected in tapping mode using a Dimension FastScan AFM (Bruker, Santa Barbara, CA, USA). Silicon nitride cantilevers with nominal spring constants of 18 N m⁻¹ were used for imaging samples in air at room temperature. A Bruker Avance III HD nanobay AX-400 spectrometer equipped with SampleXpress autosampler (Billerica, MA, USA) was used to obtain ¹³C NMR spectra of suspensions of nanoparticles in D₂O. The ACD/Spectrus processor (ACD/Labs, Toronto, Ontario, Canada) was used for manual phase correction and peak assignment.

2.4. Photostability test

A 300 mg/L (ppm) polymeric CD stock solution was made by dissolving 15 mg of polymeric CDs in 50 mL of water. Dilutions to 7.5, 18, and 30 ppm were then made, and a UV–vis extinction spectrum from 250 to 800 nm was obtained for each sample using a Varian, Inc. Cary® 50 UV–vis spectrometer (Agilent Technologies, Santa Clara, CA, USA). Before each UV–vis measurement, the quartz cuvette was rinsed with 500 μ L of the polymeric CD-containing solution, and then, 2 mL was pipetted in for analysis. Five technical replicates were recorded for each polymeric CD dilution to obtain an average spectrum and to verify that the colloidal suspension remained stable throughout the stability measurement. The linear calibration curve was used to generate a 100 mL polymeric CD-containing solution that exhibited an absorption of 0.1 at the ~345 nm peak. Once this solution was obtained, 6 mL aliquots were placed into either quartz or glass test tubes for photostability

measurements. Both the pH and emission spectrum of the remaining polymeric CDs were measured using a Orion™ 9103BNWP SemiMicro Combination Ag/AgCl pH probe (Thermo Scientific, Waltham, MA, USA) and Lumina fluorescence spectrometer (Thermo Scientific, Waltham, MA, USA), respectively. The polymeric CD-containing solutions in the glass test tubes were exposed in an RPR-100 Photochemical Rayonet Reactor® (SNEUVCo Branford, CT, USA) equipped with sixteen RMR-3500A Black Light Bulbs (>90% emission, 350 nm, 1.76 $\times 10^{17}$ quanta/s as measured with actinometry, *vida infra*). The absorption spectra for each set of polymeric CD-containing solutions were measured after 5, 10, 20, 30, 40, and 60 min of irradiation to determine the photostability. Because photodegradation is possible during the emission-excitation matrix (EEM) experiment, separate replicate samples were used for each irradiation time.

2.5. Photoluminescence quantum yield and lifetime measurements

The photoluminescence quantum yields (QY) of CACDs, the CA-P-CDs series, MACDs, and the MA-P-CDs series were determined based on protocols described in previous reports [68,69]. The extinction of each CD sample was measured with a PTI QuantaMaster 400 and then diluted to achieve an extinction value of ~0.1 340 nm. Quinine sulfate was dissolved in 0.1 M H₂SO₄ ($\phi = 0.54$) [69] and used as the standard for the quantum yield measurements (fluorimeter settings: 340 nm excitation, emission range: 350–700 nm, 1.5 nm slit width). The QY of CDs was calculated by the following equation:

$$Q_x = Q_{STD} \frac{I_x}{I_{STD}} \frac{1}{1} \frac{10}{10} \frac{OD_{STD}}{OD_x} \frac{\eta_x^2}{\eta_{STD}^2}$$

where Q stands for QY, I is the integral value of emission intensity at the excitation maximum, OD means optical density (lower than 0.1 to avoid inner filter effects), and η is the refractive index. The value of the subscript *x* identifies the polymeric CD sample while STD indicates the standard [69].

Photoluminescence lifetime measurements were performed in triplicate (extinction ~0.1) with a 375-nm laser as the excitation source (Becker&Hickl GmbH BDL 375-SMN Picosecond Diode Laser, operated at 1 MHz), slit width of 1 nm for excitation and emission, and detection at the peak wavelength of the sample. Lifetime plots were fitted with multi-exponential decay kinetics:

$$I(t) = \sum_{i=1}^{\infty} \alpha_i \exp(-t/\tau_i)$$

and the amplitude average lifetime (τ_{avg}) of each replicate is given by:

$$\tau_{avg} = \frac{\sum_{i=1}^{\infty} \alpha_i \tau_i^2}{\sum_{i=1}^{\infty} \alpha_i}$$

where α_i is the pre-exponential factor and τ_i is the lifetime of each decay [69].

2.6. Bacterial culture and polymeric carbon dot exposure

Shewanella oneidensis MR-1 (*S. oneidensis* MR-1) stock was a generous gift from the Galnick Lab at the University of Minnesota. *S. oneidensis* MR-1 were stored at 80 °C before being inoculated onto LB agar plates. The plates were incubated at 30 °C until discernible colonies were obtained. About 2–3 colonies were transferred into 10 mL LB broth. The bacterial suspension was incubated in an orbital shaker for 3–5 h and harvested before

entering stationary phase, as determined by the optical density at wavelength of 600 nm (OD_{600}). Bacteria cells were pelleted by centrifugation at 750g for 10 min, resuspended in DPBS buffer, and dispersed into HEPES buffer (2 mM HEPES and 25 mM NaCl, at pH = 7.4). The bacterial suspension was then diluted to $\sim 0.05 OD_{600}$ so that the cell density was $\sim 10^7$ cells/mL. The concentration of the polymeric CD working solution was 50 mg/mL. The subsequent nanoparticle exposure was performed by mixing the bacterial suspension with carbon dot suspension (volume ratio was 9:1, thus, the exposure concentration was 5 mg/mL), and incubated in the orbit shaker for 15 min or 1 h.

2.7. Colony counting assays (drop plate method)

To examine the possible toxic effects of phosphorus-doping into polymeric CDs (that is, comparing N-doped polymeric CDs and N, P co-doped polymeric CDs), an adapted colony counting assay (drop plate method) was used for bacterium *S. oneidensis* MR-1 [70]. As described in 2.6, A bacterial suspension of about 10^7 cells/mL ($\sim 0.05 OD_{600}$) was exposed to 5 mg/mL of polymeric CDs, followed by a 10-fold serial dilution to dilute the bacterial suspension to a proper cell density. Aliquots of 10 μ L from three dilution folds (DFs) of the exposed bacterial suspension, i.e. 10^3 , 10^4 and 10^5 , were dropped onto the surface of LB agar plates, and the agar plates were incubated at 30 °C overnight until observable colonies formed; a representative plate is shown in Fig. S10. Data from the dilution fold of 10^4 was used for further analysis as the colonies formed at this dilution fold were countable. Colony counts were transformed into

the colony-forming unit density (CFUs/mL), and normalized to the negative control by dividing CFUs of a treated sample by the average CFUs from control groups in the same experimental run, representing viability upon exposure. This calculation is done using the following equation:

$$\text{Cell Density} = \frac{1}{n} \frac{\sum_{i=1}^n x_i (\text{CFU})}{0.01 (\text{mL}) / \text{DF}}$$

$$\text{Normalized Viability} = \frac{\text{Cell Density}_{\text{TG}}}{\text{Average of Cell Density}_{\text{NC}}}$$

where NC means negative control, TG means treated group, x_i is the number of colonies counted, n indicates the number of aliquots from the same sample that were dropped onto plates, 0.01 is the volume of each aliquot (0.01 mL), and DF is the dilution fold.

3. Results and discussion

While it is currently not possible to characterize the specific atomic structure of carbon dots, this study includes an extensive array of characterization that reveals many aspects of the polymeric carbon dot structure. TEM was used to reveal the morphology of both CACDs and MACDs, as shown in Fig. 1.

Both types of polymeric CDs exhibit an approximately round shape without significant aggregation. No discernible crystal lattice was visible in either case, suggesting an amorphous nature for these polymeric CDs. Such amorphous carbon character was

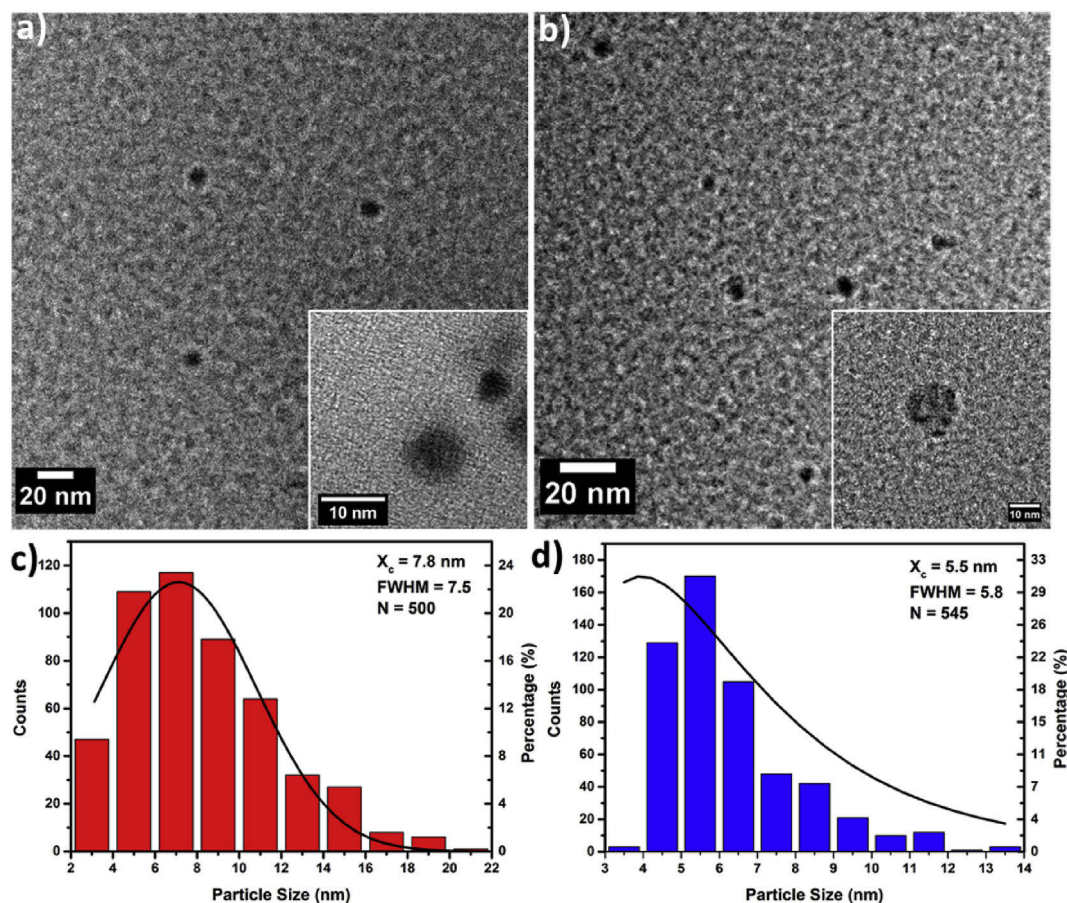


Fig. 1. TEM images of (a) CACDs and (b) MACDs (scale bar: 20 nm; inset scale: 10 nm) and particle size distributions of (c) CACDs and (d) MACDs. (A colour version of this figure can be viewed online.)

further confirmed by the broad peaks around 20 in their XRD patterns (Fig. S2) [71,72]. There may be a small amount of graphene inside, but any resulting weak diffraction signals are overwhelmed by those from amorphous carbon, so no crystalline carbon was detected via TEM or XRD. In addition, particle size analysis was performed based on CD Feret diameter from TEM images (counting 500 nanoparticles) [73]. Assuming polymeric CDs are normally distributed in size, the polymeric CD size peaks were fitted with a log-normal function to calculate the average polymeric CD size. For CACDs, the peak diameter was ~ 7.8 nm, and for MACDs, it was ~ 5.5 nm. Both are smaller than 10 nm, which is the typical size range of CDs [2,3]. Since TEM is only two-dimensional, AFM was used as well to determine the particle height distribution (z-profile). The height of CACDs and MACDs were ~ 3.7 nm and ~ 3.5 nm (Fig. S3), respectively. Both are smaller than their lateral diameter, thus, it is possible that these polymeric CDs are not perfect spheres but rather ellipsoids.

The optical properties of both polymeric CDs were examined, as shown in Fig. 2a; there are two peaks in the UV–vis spectrum of the CACDs with λ_{max} values of ~ 230 nm and ~ 350 nm. The first peak can be assigned to a $\pi-\pi^*$ transition (aromatic C=C), and the second one can be assigned to a $n-\pi^*$ transition (C–N or carboxyl) [74]. The fluorescence emission does not shift as the excitation wavelength shifts, remaining at ~ 460 nm. Unlike most reported polymeric CDs, these CACDs do not demonstrate excitation-dependent emission. The fluorescence lifetime for the CACDs was measured in triplicate using a 375 nm laser as excitation source, as shown in Fig. 2c. The lifetime trace was fitted with a multi-exponential decay function, to minimize deviation from the exponential fit function of the fluorescence lifetime of the polymeric CDs. The acceptable reduced Chi-square value ($0.9 < \chi^2 < 1.2$) and the symmetrical distribution of residuals around zero indicate a good fit. Therefore, the overall

fluorescence lifetime of CACDs is revealed by the mean value of three replicate results (τ_{avg}), that is, 11.17 ± 0.65 ns. In contrast, MACDs only showed a weak absorption feature near 350 nm (Fig. 2b), but interestingly, they exhibited excitation-dependent emission. When the excitation wavelength was adjusted from 320 nm to 400 nm, the peak of the emission spectra blue shifts from ~ 500 nm and reaches a maximum intensity at ~ 450 nm with 400 nm excitation, followed by a red-shifting emission with decreasing intensity. The fluorescence decay kinetics for MACDs are shown in Fig. 2d. The overall lifetime of MACDs was 4.77 ± 0.34 ns, shorter than that of CACDs. Furthermore, non-Raman corrected excitation emission matrices (EEM, Fig. S4) reveal information about the excited state transitions of fluorescent species. The CACD excitation:emission pairs, visualized in Fig. S4A, were easily identified as ($\lambda_{\text{ex}} = 250$ nm: $\lambda_{\text{em}} = 456.8$ nm) and ($\lambda_{\text{ex}} = 350$ nm: $\lambda_{\text{em}} = 453.9$ nm), indicating the typical excitation independence. The MACD excitation:emission pairs in Fig. S4B are not as easily isolated and have been assigned the following excitation:emission pairs: ($\lambda_{\text{ex}} = 255$ nm: $\lambda_{\text{em}} = 454.9$ nm), ($\lambda_{\text{ex}} = 340$ nm: $\lambda_{\text{em}} = 453.9$ nm), ($\lambda_{\text{ex}} = 385$ nm: $\lambda_{\text{em}} = 468.6$ nm) and ($\lambda_{\text{ex}} = 450$ nm: $\lambda_{\text{em}} = 514.5$ nm), visualizing the excitation-dependent emission. Considering the different numbers and positions of carboxyl groups within citric acid and malic acid molecules, their crosslinking patterns with ethylenediamine should be different during polymerization. As a result, the final carbonized products, the polymeric CDs, likely possess distinct structures. And so, they behave differently in terms of optical behavior. The structures of these polymeric CDs will be explored by further theoretical studies.

To delve deeper into the molecular character of these polymeric CDs, FTIR analysis was performed to characterize the functional groups within both polymeric CDs; these spectra are shown in

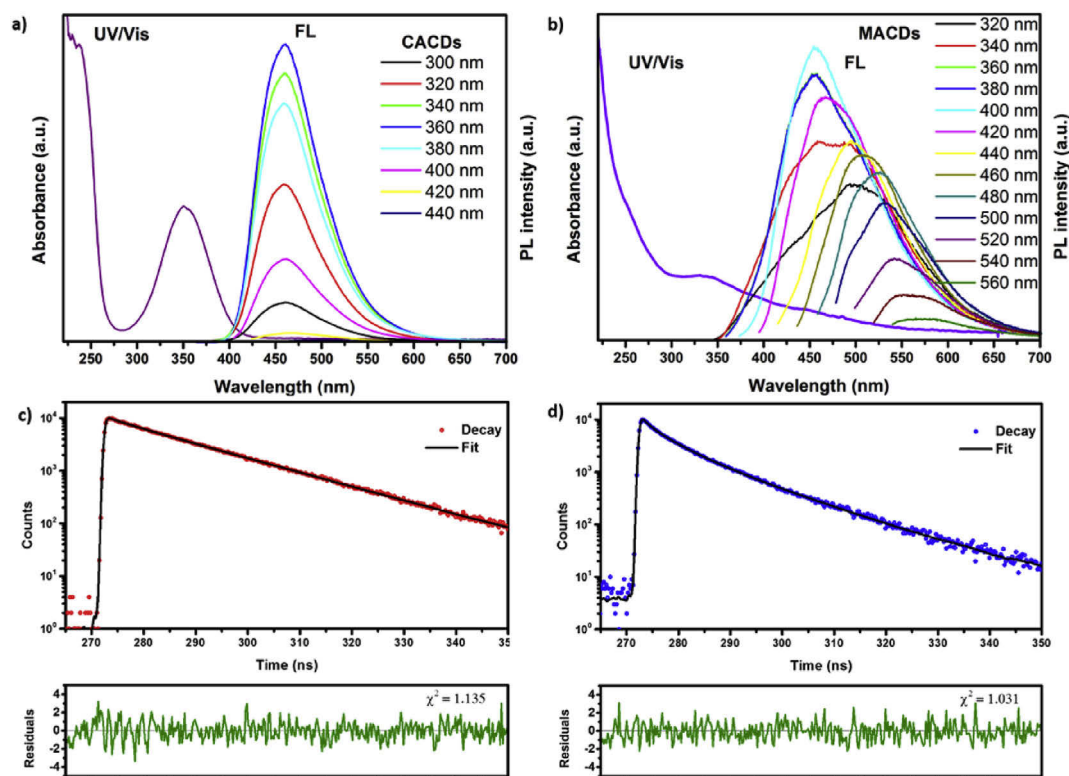


Fig. 2. Optical (UV–vis extinction and fluorescence) spectra of (a) CACDs and (b) MACDs and fluorescence lifetime traces of (c) CACDs and (d) MACDs. (A colour version of this figure can be viewed online.)

Fig. 3. The FTIR spectra of the two polymeric CDs were similar.

The broad peaks at $\sim 3200\text{ cm}^{-1}$ and $\sim 3000\text{ cm}^{-1}$ can be assigned to N–H and O–H stretching vibrations, respectively [75]. The $\sim 2900\text{ cm}^{-1}$ peak is the alkyl stretch, the main component of the carbon network. The two IR absorption bands at $\sim 1700\text{ cm}^{-1}$ and

$\sim 1640\text{ cm}^{-1}$ confirm the presence of carbonyl groups [76]. Specifically, the $\sim 1700\text{ cm}^{-1}$ peak can be attributed to carboxyl carbonyl ($-\text{COOH}$) character, and the $\sim 1640\text{ cm}^{-1}$ peak to amide carbonyl ($-\text{CO}-\text{NH}$) character [77]. The $\sim 1400\text{ cm}^{-1}$ peak confirms a C–N stretch. Moreover, ^{13}C NMR results provide a qualitative analysis of

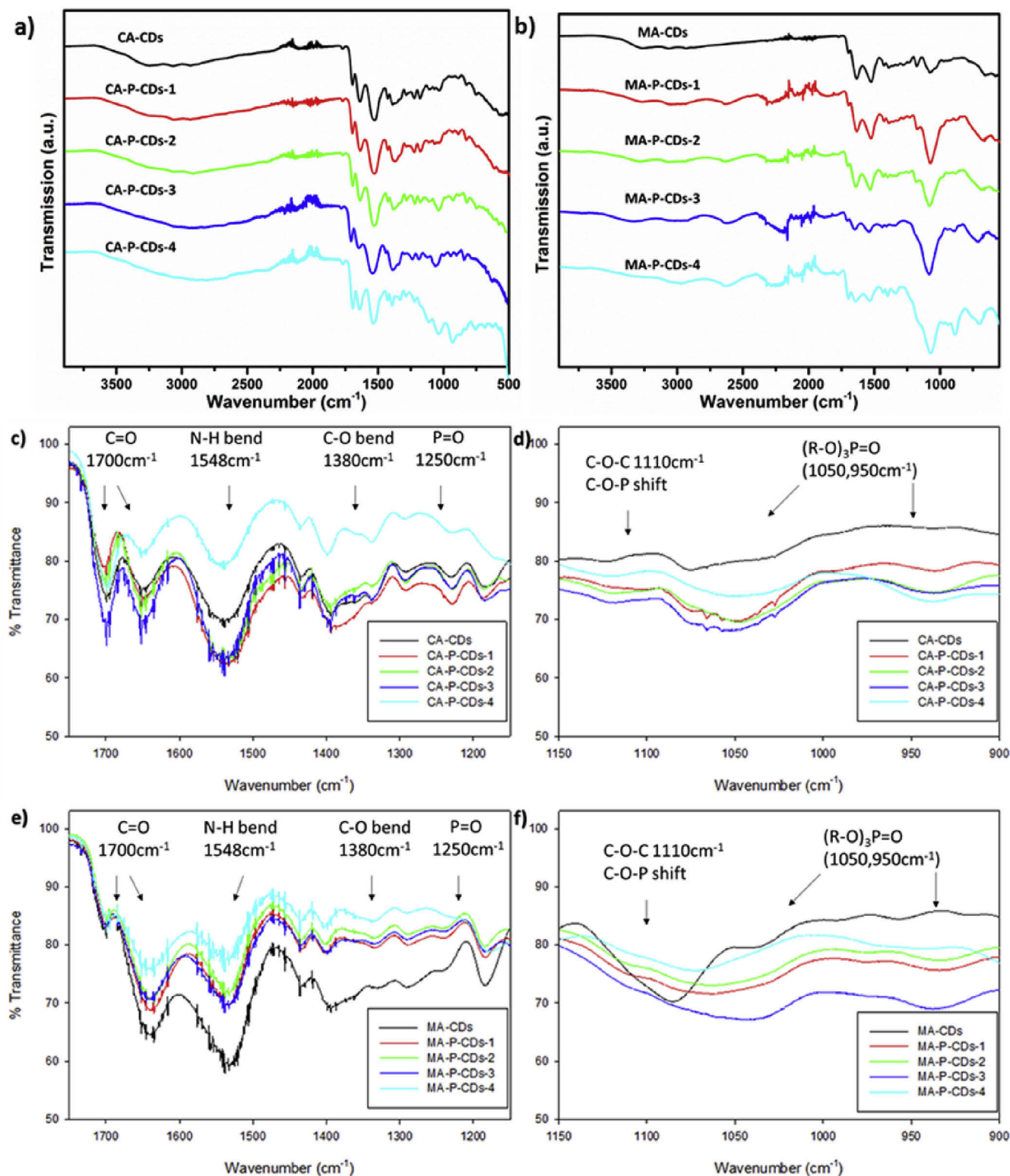


Fig. 3. FTIR spectra of (a) citric acid polymeric CD series, and (b) malic acid polymeric CD series with a detailed spectral identification of phosphorus-related peaks in citric acid polymeric CD series ((c) & (d)), and in malic acid polymeric CD series ((e) & (f)). (A colour version of this figure can be viewed online.)

the carbon hybridization state inside both the CACDs and the MACDs (Fig. S6). The ^{13}C NMR spectra reveal groups of peaks at ~ 40 ppm, ~ 70 ppm and ~ 180 ppm, respectively [78]. The ~ 40 ppm peaks can be assigned to saturated carbon (sp^3), that is, alkyl groups, R_2CH_2 , and NH_2RCH_2 groups [74,79]. The ~ 70 ppm peaks also reveal sp^3 carbon connected to an electron-withdrawing O or N atom, such as C–OH and C–N (in these cases, the peaks shift towards low field due to the electronegative effect). The CACD and CA-P-CD-4 spectra indicated the presence of two electron-withdrawing functional groups whereas the MACDs have five different electron-withdrawing functional groups. An increased number of functional groups indicates the initial hydroxyl group on the malic acid precursor molecule remains intact. The phosphorus-enriched CACDs indicate an incorporation of C=C character into the nanoparticle due to characteristic shifts at 162.40, 154.86 and 148.48 ppm. The last group at ~ 180 ppm indicates an unsaturated carbon (sp^2) present within carbonyl groups, like carboxyls ($-\text{CO}-\text{OH}$) and amides ($-\text{CO}-\text{NH}$), which means not all carbonyl groups were lost to dehydration of the precursor when crosslinked with ethylenediamine.

XPS analysis of the polymeric CDs (Fig. 4) revealed the presence of carbon, nitrogen, and oxygen. For the polymeric CDs prepared in the presence of phosphoric acid, phosphorous was also detected. The C(1s) regions for each polymeric carbon dot could be fit well using the same set of three peaks, consistent with XPS data previously obtained on polymeric CDs [44,80–85]. The peak positions of these three components are located at 288.5 eV, 286.5 eV, and 285 eV and correspond to O–C=O/O=C–N, C=O/C–N, and C=C/C–C species, respectively. These are the same species detected with IR (Fig. 3). The C(1s) region is lacking a $\pi-\pi^*$ shake-up peak at 292 eV, suggesting the absence of an extended conjugated pi-electron system. The C(1s) spectral envelopes of three of the four polymeric carbon dots (MACDs, CA-P-CDs-4, and MA-P-CDs-4) are similar; the C(1s) envelope of CACDs likely differs due to a higher concentration of C=C/C–C species. In previous work, the N(1s) XPS region of the nitrogen-containing polymeric CDs is often clearly asymmetric, indicative of a range of different nitrogen bonding environments [86–88]. In contrast, the N(1s) region of each of the four polymeric CDs analyzed in this study are very similar with a peak profile that can be fit well by a single Gaussian peak centered at ~ 400.7 eV. Although the proximity of peak positions for different nitrogen bonding environments makes an unambiguous assignment difficult, [89] the invariance of the N(1s) spectral envelope suggests that phosphorous incorporation does not lead to a significant perturbation in the chemical bonding environments of nitrogen atoms in the carbon dots. The O(1s) regions of each polymeric CD were also similar to one another, and no attempt was made to spectrally deconvolute the O(1s) regions due to the presence of a large number of bonding environments (e.g. O–C=O, C=O, P–O) and the close proximity of the peak positions. For each of the two P-doped polymeric CDs, an additional peak in the P-region was observed with a peak position (~ 134 eV) indicative of oxidized phosphorous atoms. Moreover, the level of phosphorous incorporated into the polymeric CDs could be varied by changing the usage of phosphoric acid in the synthesis (see Table S1). Hence, based on the N_{1s} , O_{1s} and P_{2p} XPS profiles, we confirm that the phosphorous doping is successful without inducing any reorganization into the original nitrogen and oxygen chemical environments of polymeric carbon dots. In addition, as XPS only reveals information about the polymeric CD surface, EDAX was used to investigate the atom percentage of each element in bulk, as shown in Fig. 5.

Clearly, the phosphorus percentage gradually increased (indicated by the arrows), up to *c.a.* 10 wt % for both polymeric carbon dots, as more phosphoric acid was used. Therefore, based on the XPS and EDAX data, we confirmed that the phosphorous doping

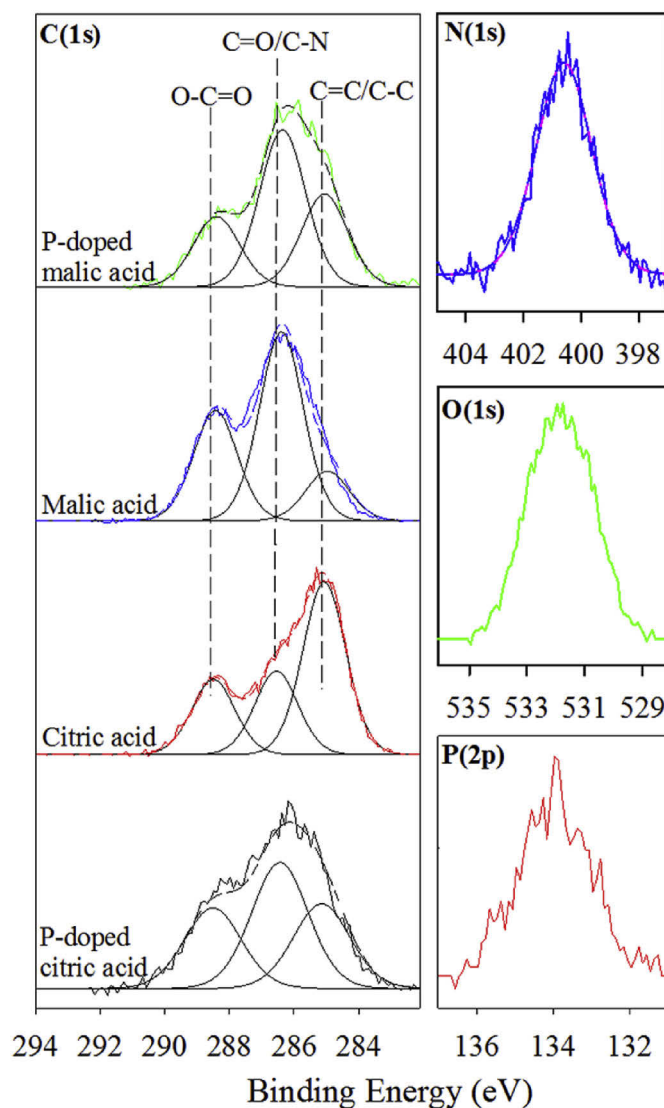


Fig. 4. XPS of C dots: (Left hand side) Comparison of the C(1s) regions for malic and citric acid carbon dots, prepared with and without phosphorous doping. (Right hand side) N(1s), O(1s) and P(2p) regions of phosphorous-doped malic acid based carbon dot (CA-P-CDs-4 and MA-P-CDs-4). (A colour version of this figure can be viewed online.)

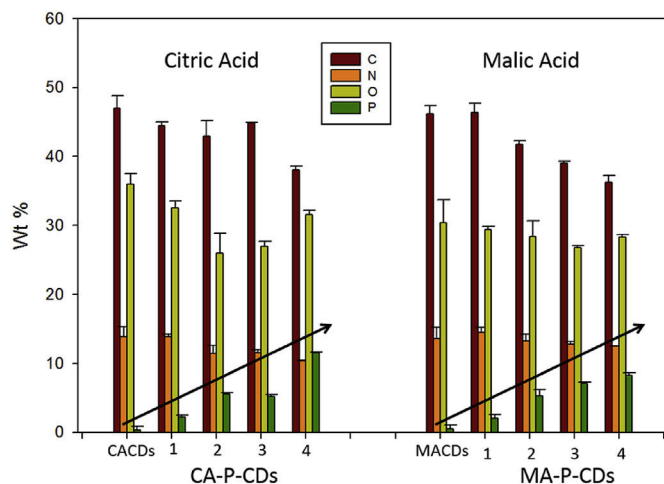


Fig. 5. EDAX element analysis of citric acid polymeric CD series (left), and malic acid polymeric CD series (right). (A colour version of this figure can be viewed online.)

was successful.

The morphology and diameter of the P-doped CACDs and MACDs were also analyzed by TEM (Figs. S7 and S8). After doping with phosphorus, both types of N, P co-doped polymeric CDs retained the quasi-spherical morphology in 2D. The average values from the size distributions for the CA-P-CDs with increasing levels of P doping were ~6.5 nm, ~6.9 nm, ~6.3 nm and ~7.1 nm, respectively. For MA-P-CDs, they were ~8.1 nm, ~7.9 nm, ~5.8 nm and ~7.3 nm, respectively. Compared to the particle diameter of the original N-doped polymeric CDs, there was no remarkable difference after adjusting the precursors to incorporate phosphorus into the polymeric CDs.

We attempted to determine the chemical features of N-doped polymeric CDs and N, P-co-doped polymeric CDs using ATR-FTIR (Fig. 3). The incorporation of the phosphorous is indicated by the shift in the 1110 cm^{-1} C–O–C vibration to a lower wavenumber due to the presence of C–O–P [79]. Furthermore, the phosphoryl (R–O)₃P = O not present in the citric acid is distinctly present in the phosphorus-rich samples around 950 cm^{-1} and 1050 cm^{-1} . In addition, the IR absorption spectra for CA-P-CDs and MA-P-CDs resembled those of CACDs and MACDs, with features attributable to carboxyl, hydroxyl and amine groups. Hence, these N, P co-doped polymeric CDs exhibited high hydrophilicity like their N-doped counterparts.

An ideal fluorophore should remain photostable for an extended period of time, so it is important to assess how doping polymeric CDs with phosphorous influences photostability. On the bench, under the influence of laboratory lighting, solutions of CDs and phosphorous-doped CDs were found to be stable over the course of at least six days, based on UV–vis analysis. To assess the effect (if any) of phosphorous doping on the photostability, it was therefore necessary to conduct accelerated photobleaching studies. This was accomplished by subjecting four of the polymeric CDs to intense visible light in a Rayonet reactor (see experimental section). Results from these studies, shown in Fig. 6, demonstrate that there was a steady decrease in absorbance over one hour of exposure, which was accompanied by a blue-shift in the peak emission. The pH of the solutions remained above 6 for the entirety of the experiments, ruling out acidic quenching [90]. The absorbance peaks were fit with a cubic baseline and subsequently a Gaussian function as

detailed in Tan et al. (Fig. S12). [91]. For the first 40 min, CA-P-CDs-4 exhibited higher, but not statistically different, photostability than the CACDs. The MA-P-CDs-4 demonstrated a statistically significant ~25% increase in photostability compared to MACDs after 60 min exposure. Thus Fig. 6 demonstrates that distinct advantages in photostability are gained by doping the MACDs with phosphorous. The overall stability trend with these four samples after one hour exposure was determined to be: MA-P-CDs-4 > MACDs > CACDs > CA-P-CDs-4.

Previous accelerated photobleaching studies of CDs have typically been conducted by measuring changes in the photoluminescence (PL) yield under a wide range of different conditions (e.g. exposure to the white light from a Xe lamp, continuous irradiation at 360 nm), where the incident photon flux is not reported [92–96]. Consequently, a direct quantitative comparison of the results from this investigation to previous photobleaching studies of CDs is not possible. However, in general, photostability is found to depend on the synthetic route used to prepare the CDs. Specifically, crystalline CDs prepared by a “top-down” approach (e.g. by exfoliating carbon nitride using acid) are extremely photostable even when exposed to intense light sources (e.g. no change in PL after irradiation with a 365 nm UV lamp for 12 h) [94]. In contrast, CDs prepared using a “bottom-up” approach (typically hydrothermally or by using microwaves) are more susceptible to photobleaching, an effect ascribed to the presence of a greater number of surface defects [93,96]. Results from the present study are therefore in qualitative agreement with this general trend.

The high QY of the CACDs was in concurrence with literature values [6,8,46]. After doping with different levels of phosphorous, the QY of doped CACDs was maintained around 40% (Table S2). Specifically, the QY is 40.98% for CA-P-CDs-1, 39.29% for CA-P-CDs-2, 35.56% for CA-P-CDs-3, and 44.23% for CA-P-CDs-4. The citric acid polymeric CDs are found to be much more efficient at conversion of absorbed photons with 340 nm laser excitation than the malic acid polymeric CDs. The most prominent excitation, however, occurs at 385 nm for the MACDs. The MACDs were found to have a quantum yield closer to that of tryptophan (~14%) [69]. The QY of MACD series remained c.a. 10% after P-doping (Table S2), that is, 15.56% for MA-P-CDs-1, 11.58% for MA-P-CDs-2, 10.19% for MA-P-CDs-3, and 11.99% for MA-P-CDs-4. The MACD series may have lower quantum yields due to the multiple pathways for relaxation shown in the EEM in Fig. S4B and D. The fluorescence lifetimes, τ , of citric acid polymeric CDs are about two times longer than those of malic acid polymeric CDs (Table S2). The lifetimes have decreased after doping phosphorous into CACDs, but there was no such effect for P-doped MACDs (Fig. S9).

With luminescence and photostability properties of the new polymeric CDs looking promising, nanoparticle toxicity was considered since one proposed advantage of polymeric CDs over traditional QDs lies in their likely biocompatibility. Fig. 7 describes the toxicity results of polymeric CDs towards the model bacterium, *S. oneidensis* MR-1, as measured by a colony counting assay (drop plate method).

Statistical analysis was performed using one-way ANOVA, followed by post-hoc Tukey's multiple comparisons tests (GraphPad Prism software, La Jolla, CA). All values plotted are the mean \pm standard error of mean, and statistical significance is indicated using asterisks (* $p < 0.05$, ** $p < 0.01$, *** $p < 0.001$ and **** $p < 0.0001$). The results show that, in most cases, neither N-doped polymeric CDs nor N, P co-doped polymeric CDs exhibit a toxic effect; on the contrary, the bacteria formed more colonies than the negative control (untreated) samples in some cases. This increased colony formation suggests that *S. oneidensis* MR-1 can potentially use polymeric CDs as their carbon nutrient source. In fact, it is known that *S. oneidensis* MR-1 performs a standard

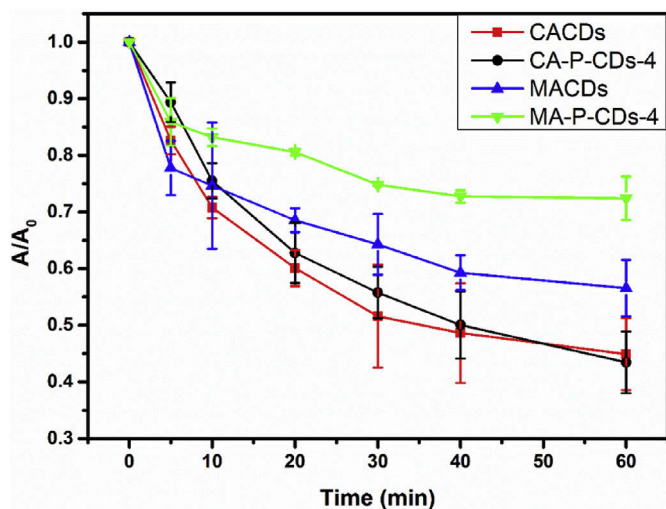


Fig. 6. Photostability of the CACDs, CA-P-CDs-4, MACDs and MA-P-CDs-4. Photostability was determined by measuring the change in the absorbance (A/A_0) at 350 nm as a function of CD exposure to the intense visible light generated in a Rayonet (see experimental section). (A colour version of this figure can be viewed online.)

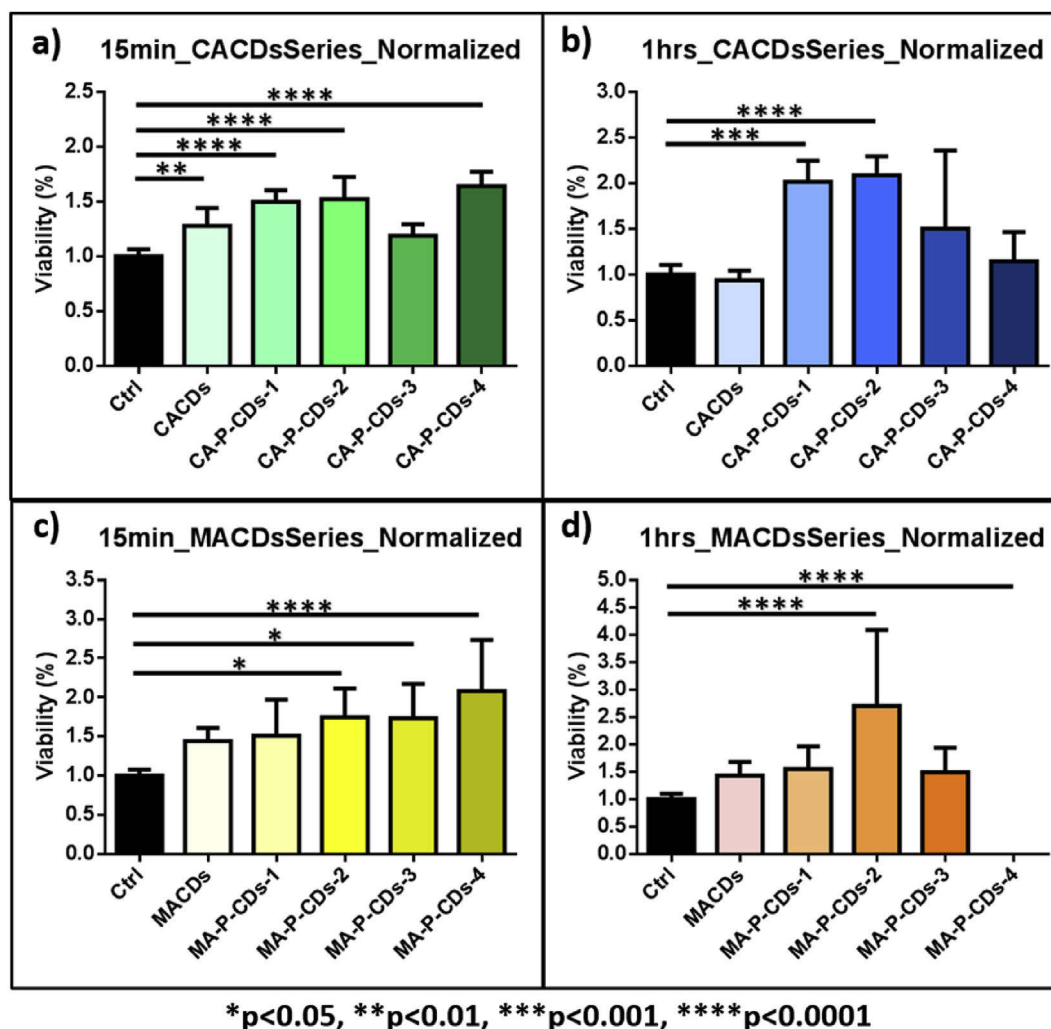


Fig. 7. Colony counting assay results of citric acid polymeric CDs after (a) 15-min exposure and (b) one-hour exposure, and results of malic acid polymeric CDs after (c) 15-min exposure and (d) 1-h exposure (Error bars indicate standard deviation, and for simplicity, only the positive half of each error bar is shown). (A colour version of this figure can be viewed online.)

tricarboxylic acid (TCA) cycle for carbon metabolism under aerobic growth [97] wherein citric acid and malate anions play a role. However, neither genomic prediction nor experimental evidence have previously demonstrated that this bacterium can utilize citric acid or malic acid as a carbon source [98]. It is possible that other components in the polymeric CDs, such as phosphorus or unknown by-products from the synthesis, promote bacterial colony formation. It is worth noting that the MA-P-CDs-4 (malic acid carbon dots doped with the highest amount of phosphorus) showed extremely high bacterial toxicity, eradicating almost the whole bacterial population. Recall from Fig. 6, doping the malic acid samples with phosphorous gained an advantage in photostability which may not be favorable when compared to the toxic response seen in the *S. oneidensis* MR-1 over one hour exposure. It is worth noting, however, that the threshold to toxicity is quite high at 5000 mg/L in a concentrated (300 μ L) solution. This high concentration would be too bright for a detector in a confocal scanner and would be an impractical working solution concentration for bio-imaging. It is also important to note that the need for something to be illuminated over an hour in a microscope may be unnecessary. Notwithstanding, the gains in photostability and lower quantum yield demonstrate phosphorous doping of malic acid might not be worth the acute toxicity exhibited in *S. oneidensis* MR-1. Future

studies on metabolomics could provide insight into the stress imposed upon this organism by the high concentration of particles. Other model organisms would also give a well-rounded picture of acute toxicity. Finally, it may be important to look at the photo-degraded polymeric carbon dots to assess if the photoproducts are, in and of themselves, toxic. It was initially suspected that such toxicity was a result of light-induced polymeric CD degradation, since the exposure was done under lab light, and the toxicity was only apparent after one hour exposure; thus, another two sets of experiments were set up to investigate this possibility. Results showed that lab light was not the source of the high toxicity of MA-P-CDs-4 (Fig. S11). The source of this repeatable high toxicity after one hour exposure is the subject of ongoing investigation. In general, most of the polymeric CDs were not at all toxic towards the *S. oneidensis* MR-1 even at high doses (5 mg/mL), showing that polymeric CDs are quite benign. Thus, the non-toxic polymeric CDs can be used for further bio-imaging and bio-sensing studies.

4. Conclusion

Polymeric CDs display reproducible, highly marketable luminescence properties that are influenced by chemical composition. In this work, citric acid and malic acid were used as carbon sources

to generate N-doped polymeric CDs (using ethylenediamine as the nitrogen source). Furthermore, various amounts of phosphorus were introduced into these polymeric CDs, resulting in N, P-co-doped polymeric CDs. These doped polymeric CDs were great to systematically and quantitatively analyze the impact of phosphorus doping on emission properties, photostability, and toxicity; the results reveal that there is no remarkable influence after doping with phosphorus in terms of quantum yield or lifetime. The starting material with three carboxylic acid groups was found to be a better performing polymeric carbon dot with higher quantum yield and longer fluorescent lifetime compared to the starting material with two carboxylic acid groups. By contrast, the N, P-co-doped malic acid polymeric CDs may show an advantage over N, P-co-doped citric acid polymeric CDs and N-doped polymeric CDs in terms of photostability under 350 nm UV exposure. Any advantages accrued in photostability are diminished by the toxicity results. Lastly, to assess the possibility that luminescent CDs may be a viable replacement for toxic heavy metal-based quantum dots in a variety of applications, the bacterial toxicity of these doped polymeric CDs was evaluated using *S. oneidensis* MR-1 as a model microorganism. The polymeric CDs exhibited no inhibition in bacterial viability in most cases, and in some cases, even facilitated bacterial growth, making polymeric CDs a potentially eco-friendly fluorescent material with a wide range of potential applications.

Acknowledgement

This work was supported by the National Science Foundation Center for Chemical Innovation Program Grant No. CHE-1503408 under the Center for Sustainable Nanotechnology. Parts of this work, including XPS and TEM characterization, were carried out in the Characterization Facility, University of Minnesota, which receives partial support from the MRSEC program. We would like to thank the Materials Characterization Facility at Johns Hopkins University Whiting School of Engineering for use of their facilities.

Appendix A. Supplementary data

Supplementary data related to this article can be found at <https://doi.org/10.1016/j.carbon.2017.12.004>.

References

- [1] X. Xu, R. Ray, Y. Gu, H.J. Ploehn, L. Gearheart, K. Raker, W.A. Scrivens, Electrophoretic analysis and purification of fluorescent single-walled carbon nanotube fragments, *J. Am. Chem. Soc.* 126 (40) (2004) 12736–12737.
- [2] V. Georgakilas, J.A. Perman, J. Tucek, R. Zboril, Broad family of carbon nanomaterials: classification, chemistry, and applications of fullerenes, carbon dots, nanotubes, graphene, nanodiamonds, and combined superstructures, *Chem. Rev.* 115 (11) (2015) 4744–4822.
- [3] G. Hong, S. Diao, A.L. Antaris, H. Dai, Carbon nanomaterials for biological imaging and nanomedical therapy, *Chem. Rev.* 115 (19) (2015) 10816–10906.
- [4] S.Y. Lim, W. Shen, Z. Gao, Carbon quantum dots and their applications, *Chem. Soc. Rev.* 44 (1) (2015) 362–381.
- [5] W.W.-W. Hsiao, Y.Y. Hui, P.-C. Tsai, H.-C. Chang, Fluorescent nanodiamond: a versatile tool for long-term cell tracking, super-resolution imaging, and nanoscale temperature sensing, *Acc. Chem. Res.* 49 (3) (2016) 400–407.
- [6] S. Zhu, Q. Meng, L. Wang, J. Zhang, Y. Song, H. Jin, K. Zhang, H. Sun, H. Wang, B. Yang, Highly photoluminescent carbon dots for multicolor patterning, sensors, and bioimaging, *Angew. Chem. Int. Ed.* 52 (14) (2013) 3953–3957.
- [7] Z. Luo, G. Qi, K. Chen, M. Zou, L. Yuwen, X. Zhang, W. Huang, L. Wang, Microwave-assisted preparation of white fluorescent graphene quantum dots as a novel phosphor for enhanced white-light-emitting diodes, *Adv. Funct. Mater.* 26 (16) (2016) 2739–2744.
- [8] X. Zhai, P. Zhang, C. Liu, T. Bai, W. Li, L. Dai, W. Liu, Highly luminescent carbon nanodots by microwave-assisted pyrolysis, *Chem. Commun.* 48 (64) (2012) 7955–7957.
- [9] Y. Li, C. Luo, C. Jiang, R. Huang, Y. Wang, H. Peng, J. Travas-Sejdic, Luminescent carbon nanoparticles as a donor for the FRET-based detection of oligonucleotide hybridization, *RSC Adv.* 4 (48) (2014) 25201–25204.
- [10] C.-I. Weng, H.-T. Chang, C.-H. Lin, Y.-W. Shen, B. Unnikrishnan, Y.-J. Li, C.-C. Huang, One-step synthesis of bifunctional carbon quantum dots for bacterial labeling, *Biosens. Bioelectron.* 68 (0) (2015) 1–6.
- [11] S. Chandra, D. Laha, A. Pramanik, A. Ray Chowdhuri, P. Karmakar, S.K. Sahu, Synthesis of highly fluorescent nitrogen and phosphorus doped carbon dots for the detection of Fe³⁺ ions in cancer cells, *Luminescence* 31 (1) (2016) 81–87.
- [12] Y. Gong, B. Yu, W. Yang, X. Zhang, Phosphorus, and nitrogen co-doped carbon dots as a fluorescent probe for real-time measurement of reactive oxygen and nitrogen species inside macrophages, *Biosens. Bioelectron.* 79 (Suppl. C) (2016) 822–828.
- [13] S. Pang, Y. Zhang, C. Wu, S. Feng, Fluorescent carbon dots sensor for highly sensitive detection of guanine, *Sensors Actuator. B Chem.* 222 (2016) 857–863.
- [14] B. Shi, Y. Su, L. Zhang, M. Huang, R. Liu, S. Zhao, Nitrogen and phosphorus Co-Doped carbon nanodots as a novel fluorescent probe for highly sensitive detection of Fe³⁺ in human serum and living cells, *ACS Appl. Mater. Interfaces* 8 (17) (2016) 10717–10725.
- [15] W. Wang, Y. Li, L. Cheng, Z. Cao, W. Liu, Water-soluble and phosphorus-containing carbon dots with strong green fluorescence for cell labeling, *J. Mater. Chem. B* 2 (1) (2014) 46–48.
- [16] T. Feng, X. Ai, G. An, P. Yang, Y. Zhao, Charge-convertible carbon dots for imaging-guided drug delivery with enhanced in Vivo cancer therapeutic efficiency, *ACS Nano* 10 (4) (2016) 4410–4420.
- [17] X. Gong, Q. Zhang, Y. Gao, S. Shuang, M.M.F. Choi, C. Dong, Phosphorus and nitrogen dual-doped hollow carbon dot as a nanocarrier for doxorubicin delivery and biological imaging, *ACS Appl. Mater. Interfaces* 8 (18) (2016) 11288–11297.
- [18] F. Zhang, Y. Wang, Y. Miao, Y. He, Y. Yang, X. Liu, Optimal nitrogen and phosphorus codoping carbon dots towards white light-emitting device, *Appl. Phys. Lett.* 109 (8) (2016), 083103.
- [19] H. Li, X. He, Z. Kang, H. Huang, Y. Liu, J. Liu, S. Lian, C.H.A. Tsang, X. Yang, S.-T. Lee, Water-Soluble fluorescent carbon quantum dots and photocatalyst design, *Angew. Chem. Int. Ed.* 49 (26) (2010) 4430–4434.
- [20] H. Ming, Z. Ma, Y. Liu, K. Pan, H. Yu, F. Wang, Z. Kang, Large scale electrochemical synthesis of high quality carbon nanodots and their photocatalytic property, *Dalton Trans.* 41 (31) (2012) 9526–9531.
- [21] B.Y. Yu, S.-Y. Kwak, Carbon quantum dots embedded with mesoporous hematite nanospheres as efficient visible light-active photocatalysts, *J. Mater. Chem.* 22 (17) (2012) 8345–8353.
- [22] S.J. Zhu, Y.B. Song, X.H. Zhao, J.R. Shao, J.H. Zhang, B. Yang, The photoluminescence mechanism in carbon dots (graphene quantum dots, carbon nanodots, and polymer dots): current state and future perspective, *Nano Res.* 8 (2) (2015) 355–381.
- [23] Y.-P. Sun, B. Zhou, Y. Lin, W. Wang, K.A.S. Fernando, P. Pathak, M.J. Meziani, B.A. Harruff, X. Wang, H. Wang, P.G. Luo, H. Yang, M.E. Kose, B. Chen, L.M. Veca, S.-Y. Xie, Quantum-sized carbon dots for bright and colorful photoluminescence, *J. Am. Chem. Soc.* 128 (24) (2006) 7756–7757.
- [24] L. Bao, Z.-L. Zhang, Z.-Q. Tian, L. Zhang, C. Liu, Y. Lin, B. Qi, D.-W. Pang, Electrochemical tuning of luminescent carbon nanodots: from preparation to luminescence mechanism, *Adv. Mater.* 23 (48) (2011) 5801–5806.
- [25] J. Peng, W. Gao, B.K. Gupta, Z. Liu, R. Romero-Aburto, L. Ge, L. Song, L.B. Alemany, X. Zhan, G. Gao, S.A. Vithayathil, B.A. Kaiparettu, A.A. Marti, T. Hayashi, J.-J. Zhu, P.M. Ajayan, Graphene quantum dots derived from carbon fibers, *Nano Lett.* 12 (2) (2012) 844–849.
- [26] D.B. Shinde, V.K. Pillai, Electrochemical preparation of luminescent graphene quantum dots from multiwalled carbon nanotubes, *Chem. – A Eur. J.* 18 (39) (2012) 12522–12528.
- [27] A. Zhao, Z. Chen, C. Zhao, N. Gao, J. Ren, X. Qu, Recent advances in bio-applications of C-dots, *Carbon* 85 (2015) 309–327.
- [28] Y. Wang, A. Hu, Carbon quantum dots: synthesis, properties and applications, *J. Mater. Chem. C* 2 (34) (2014) 6921–6939.
- [29] X. Li, S.P. Lau, L. Tang, R. Ji, P. Yang, Sulphur doping: a facile approach to tune the electronic structure and optical properties of graphene quantum dots, *Nanoscale* 6 (10) (2014) 5323–5328.
- [30] S. Sarkar, K. Das, M. Ghosh, P.K. Das, Amino acid functionalized blue and phosphorous-doped green fluorescent carbon dots as bioimaging probe, *RSC Adv.* 5 (81) (2015) 65913–65921.
- [31] H.-X. Wang, Z. Yang, Z.-G. Liu, J.-Y. Wan, J. Xiao, H.-L. Zhang, Facile preparation of bright-fluorescent soft materials from small organic molecules, *Chem. – A Eur. J.* 22 (24) (2016) 8096–8104.
- [32] A.M. Schwenke, S. Hoepfner, U.S. Schubert, Synthesis and modification of carbon nanomaterials utilizing microwave heating, *Adv. Mater.* 27 (28) (2015) 4113–4141.
- [33] M.B. Gawande, S.N. Shelke, R. Zboril, R.S. Varma, Microwave-assisted chemistry: synthetic applications for rapid assembly of nanomaterials and organics, *Acc. Chem. Res.* 47 (4) (2014) 1338–1348.
- [34] C.O. Kappe, D. Dallinger, S.S. Murphree, *Experimental Protocols, Practical Microwave Synthesis for Organic Chemists*, Wiley-VCH Verlag GmbH & Co. KGaA, 2009, pp. 203–290.
- [35] L. Tang, R. Ji, X. Cao, J. Lin, H. Jiang, X. Li, K.S. Teng, C.M. Luk, S. Zeng, J. Hao, S.P. Lau, Deep ultraviolet photoluminescence of water-soluble self-passivated graphene quantum dots, *ACS Nano* 6 (6) (2012) 5102–5110.
- [36] Q. Wang, H. Zheng, Y. Long, L. Zhang, M. Gao, W. Bai, Microwave–hydrothermal synthesis of fluorescent carbon dots from graphite

- oxide. Carbon 49 (9) (2011) 3134–3140.
- [37] P. Zhang, W. Li, X. Zhai, C. Liu, L. Dai, W. Liu, A facile and versatile approach to biocompatible “fluorescent polymers” from polymerizable carbon nanodots, Chem. Commun. 48 (84) (2012) 10431–10433.
- [38] Y. Song, W. Shi, W. Chen, X. Li, H. Ma, Fluorescent carbon nanodots conjugated with folic acid for distinguishing folate-receptor-positive cancer cells from normal cells, J. Mater. Chem. 22 (25) (2012) 12568–12573.
- [39] S. Chandra, P. Das, S. Bag, D. Laha, P. Pramanik, Synthesis, functionalization and bioimaging applications of highly fluorescent carbon nanoparticles, Nanoscale 3 (4) (2011) 1533–1540.
- [40] Y.-C. Lin, C.-Y. Lin, P.-W. Chiu, Controllable graphene N-doping with ammonia plasma, Appl. Phys. Lett. 96 (13) (2010), 133110.
- [41] L. Ma, H. Hu, L. Zhu, J. Wang, Boron and nitrogen doping induced half-metallicity in zigzag triwing graphene nanoribbons, J. Phys. Chem. C 115 (14) (2011) 6195–6199.
- [42] H. Liu, Y. Liu, D. Zhu, Chemical doping of graphene, J. Mater. Chem. 21 (10) (2011) 3335–3345.
- [43] X. Dong, Y. Su, H. Geng, Z. Li, C. Yang, X. Li, Y. Zhang, Fast one-step synthesis of N-doped carbon dots by pyrolyzing ethanolamine, J. Mater. Chem. C 2 (36) (2014) 7477–7481.
- [44] W. Lu, X. Gong, M. Nan, Y. Liu, S. Shuang, C. Dong, Comparative study for N and S doped carbon dots: synthesis, characterization and applications for Fe³⁺ probe and cellular imaging, Anal. Chim. Acta 898 (2015) 116–127.
- [45] F. Arcudi, L. Đorđević, M. Prato, Synthesis, separation, and characterization of small and highly fluorescent nitrogen-doped carbon NanoDots, Angew. Chem. Int. Ed. 55 (6) (2016) 2107–2112.
- [46] Y. Dong, H. Pang, H.B. Yang, C. Guo, J. Shao, Y. Chi, C.M. Li, T. Yu, Carbon-based dots Co-doped with nitrogen and sulfur for high quantum yield and excitation-independent emission, Angew. Chem. Int. Ed. 52 (30) (2013) 7800–7804.
- [47] X. Shan, L. Chai, J. Ma, Z. Qian, J. Chen, H. Feng, B-doped carbon quantum dots as a sensitive fluorescence probe for hydrogen peroxide and glucose detection, Analyst 139 (10) (2014) 2322–2325.
- [48] S. Jahan, F. Mansoor, S. Naz, J. Lei, S. Kanwal, Oxidative synthesis of highly fluorescent boron/nitrogen Co-Doped carbon nanodots enabling detection of photosensitizer and carcinogenic dye, Anal. Chem. 85 (21) (2013) 10232–10239.
- [49] M.K. Barman, B. Jana, S. Bhattacharyya, A. Patra, Photophysical properties of doped carbon dots (N, P, and B) and their influence on electron/hole transfer in carbon dots–nickel (II) phthalocyanine conjugates, J. Phys. Chem. C 118 (34) (2014) 20034–20041.
- [50] H. Li, F.-Q. Shao, S.-Y. Zou, Q.-J. Yang, H. Huang, J.-J. Feng, A.-J. Wang, Microwave-assisted synthesis of N,P-doped carbon dots for fluorescent cell imaging, Microchim. Acta 183 (2) (2016) 821–826.
- [51] X. Sun, C. Bruckner, Y. Lei, One-pot and ultrafast synthesis of nitrogen and phosphorus co-doped carbon dots possessing bright dual wavelength fluorescence emission, Nanoscale 7 (41) (2015) 17278–17282.
- [52] W. Wu, L. Zhan, W. Fan, J. Song, X. Li, Z. Li, R. Wang, J. Zhang, J. Zheng, M. Wu, H. Zeng, Cu–N dopants boost electron transfer and photooxidation reactions of carbon dots, Angew. Chem. Int. Ed. 54 (22) (2015) 6540–6544.
- [53] F. Li, C. Liu, J. Yang, Z. Wang, W. Liu, F. Tian, Mg/N double doping strategy to fabricate extremely high luminescent carbon dots for bioimaging, RSC Adv. 4 (7) (2014) 3201–3205.
- [54] X.Y. Ren, X.X. Yuan, Y.P. Wang, C.L. Liu, Y. Qin, L.P. Guo, L.H. Liu, Facile preparation of Gd³⁺ doped carbon quantum dots: photoluminescence materials with magnetic resonance response as magnetic resonance/fluorescence bimodal probes, Opt. Mater. 57 (2016) 56–62.
- [55] D. Sun, R. Ban, P.-H. Zhang, G.-H. Wu, J.-R. Zhang, J.-J. Zhu, Hair fiber as a precursor for synthesizing sulfur- and nitrogen-co-doped carbon dots with tunable luminescence properties, Carbon 64 (2013) 424–434.
- [56] L. Zhang, Z. Xia, Mechanisms of oxygen reduction reaction on nitrogen-doped graphene for fuel cells, J. Phys. Chem. C 115 (22) (2011) 11170–11176.
- [57] H. Wang, P. Sun, S. Cong, J. Wu, L. Gao, Y. Wang, X. Dai, Q. Yi, G. Zou, Nitrogen-doped carbon dots for “green” quantum dot solar cells, Nanoscale Res. Lett. 11 (1) (2016), 27–27.
- [58] Y. Guo, Z. Wang, H. Shao, X. Jiang, Hydrothermal synthesis of highly fluorescent carbon nanoparticles from sodium citrate and their use for the detection of mercury ions, Carbon 52 (2013) 583–589.
- [59] S.N. Baker, G.A. Baker, Luminescent carbon nanodots: emergent nanolights, Angew. Chem. Int. Ed. 49 (38) (2010) 6726–6744.
- [60] A. Xiao, C. Wang, J. Chen, R. Guo, Z. Yan, J. Chen, Carbon and metal quantum dots toxicity on the microalgae *Chlorella pyrenoidosa*, Ecotoxicol. Environ. Saf. 133 (2016) 211–217.
- [61] W. Liu, J. Yao, J. Jin, J. Ma, K. Masakorala, Microbial toxicity of a type of carbon dots to *Escherichia coli*, Arch. Environ. Contam. Toxicol. 69 (4) (2015) 506–514.
- [62] P.H. Raven, K.A. Mason, G.B. Johnson, J.B. Losos, S.R. Singer, Biology, McGraw-Hill, 2011.
- [63] L. Shi, K.M. Rosso, T.A. Clarke, D.J. Richardson, J.M. Zachara, J.K. Fredrickson, Molecular underpinnings of Fe(III) oxide reduction by *Shewanella oneidensis* MR-1, Front. Microbiol. 3 (2012).
- [64] J.M. Janda, S.L. Abbott, The genus *Shewanella*: from the briny depths below to human pathogen, Crit. Rev. Microbiol. 40 (4) (2014) 293–312.
- [65] I.L. Gunsolus, M.P. Mousavi, K. Hussein, P. Bühlmann, C.L. Haynes, Effects of humic and fulvic acids on silver nanoparticle stability, dissolution, and toxicity, Environ. Sci. Technol. 49 (13) (2015) 8078–8086.
- [66] Z.V. Feng, I.L. Gunsolus, T.A. Qiu, K.R. Hurlley, L.H. Nyberg, H. Frew, K.P. Johnson, A.M. Vartanian, L.M. Jacob, S.E. Lohse, M.D. Torelli, R. Hamers, C. Murphy, C. Haynes, Impacts of gold nanoparticle charge and ligand type on surface binding and toxicity to gram-negative and gram-positive bacteria, Chem. Sci. 6 (2015) 5186–5196.
- [67] M.N. Hang, I.L. Gunsolus, H. Wayland, E.S. Melby, A.C. Mensch, K.R. Hurlley, J.A. Pedersen, C.L. Haynes, R.J. Hamers, Impact of nanoscale lithium nickel manganese cobalt oxide (NMC) on the bacterium *Shewanella oneidensis* MR-1, Chem. Mater. 28 (4) (2016) 1092–1100.
- [68] S. Sahu, B. Behera, T.K. Maiti, S. Mohapatra, Simple one-step synthesis of highly luminescent carbon dots from orange juice: application as excellent bio-imaging agents, Chem. Commun. 48 (70) (2012) 8835–8837.
- [69] J.R. Lakowicz, Principles of Fluorescence Spectroscopy, Springer Science & Business Media, 2013.
- [70] T.A. Qiu, M.D. Torelli, A.M. Vartanian, N.B. Rackstraw, J.T. Buchman, L.M. Jacob, C.J. Murphy, R.J. Hamers, C.L. Haynes, Quantification of free polyelectrolytes present in colloidal suspension, revealing a source of toxic responses for polyelectrolyte-wrapped gold nanoparticles, Anal. Chem. 89 (3) (2017) 1823–1830.
- [71] M.P. Sk, A. Jaiswal, A. Paul, S.S. Ghosh, A. Chattopadhyay, Presence of amorphous carbon nanoparticles in food caramels, Sci. Rep. 2 (2012) 383.
- [72] A.L. Himaja, P.S. Karthik, S.P. Singh, Carbon dots: the newest member of the carbon nanomaterials family, Chem. Rec. 15 (3) (2015) 595–615.
- [73] H.G. Merkus, Particle Size Measurements: Fundamentals, Practice, Quality, Springer Science & Business Media, 2009.
- [74] D. Pavia, G. Lampman, G. Kriz, J. Vyvyan, Introduction to Spectroscopy, Cengage Learning, 2008.
- [75] K. Jiang, S. Sun, L. Zhang, Y. Lu, A. Wu, C. Cai, H. Lin, Red, green, and blue luminescence by carbon dots: full-color emission tuning and multicolor cellular imaging, Angew. Chem. Int. Ed. 54 (18) (2015) 5360–5363.
- [76] W. Li, Z. Zhang, B. Kong, S. Feng, J. Wang, L. Wang, J. Yang, F. Zhang, P. Wu, D. Zhao, Simple and green synthesis of nitrogen-doped photoluminescent carbonaceous nanospheres for bioimaging, Angew. Chem. Int. Ed. 52 (31) (2013) 8151–8155.
- [77] Y. Zhang, X. Liu, Y. Fan, X. Guo, L. Zhou, Y. Lv, J. Lin, One-step microwave synthesis of N-doped hydroxyl-functionalized carbon dots with ultra-high fluorescence quantum yields, Nanoscale 8 (33) (2016) 15281–15287.
- [78] D.L. Pavia, G.M. Lampman, G.S. Kriz, Introduction to Spectroscopy: a Guide for Students of Organic Chemistry, Harcourt College Publishers, 2001.
- [79] R.M. Silverstein, F.X. Webster, D.J. Kiemle, D.L. Bryce, Spectrometric Identification of Organic Compounds, John Wiley & Sons, 2014.
- [80] H. Dang, L.-K. Huang, Y. Zhang, C.-F. Wang, S. Chen, Large-scale ultrasonic fabrication of white fluorescent carbon dots, Ind. Eng. Chem. Res. 55 (18) (2016) 5335–5341.
- [81] Y. Zhang, Y. Wang, Y. Guan, L. Feng, Uncovering the pKa dependent fluorescence quenching of carbon dots induced by chlorophenols, Nanoscale 7 (14) (2015) 6348–6355.
- [82] M. Algarra, M. Perez-Martin, M. Cifuentes-Rueda, J. Jimenez-Jimenez, J.C.G. Esteves da Silva, T.J. Bandoz, E. Rodriguez-Castellon, J.T. Lopez Navarrete, J. Casado, Carbon dots obtained using hydrothermal treatment of formaldehyde. Cell imaging in vitro, Nanoscale 6 (15) (2014) 9071–9077.
- [83] J. Liu, X. Ge, L. Sun, R. Wei, J. Liu, L. Shi, Light modulation (vis-NIR region) based on lanthanide complex-functionalized carbon dots, RSC Adv. 6 (53) (2016) 47427–47433.
- [84] F.A. Permatasari, A.H. Aimon, F. Iskandar, T. Ogi, K. Okuyama, Role of C–N configurations in the photoluminescence of graphene quantum dots synthesized by a hydrothermal route, Sci. Rep. 6 (2016) 21042.
- [85] Q. Hu, M.C. Paa, Y. Zhang, X. Gong, L. Zhang, D. Lu, Y. Liu, Q. Liu, J. Yao, M.M.F. Choi, Green synthesis of fluorescent nitrogen/sulfur-doped carbon dots and investigation of their properties by HPLC coupled with mass spectrometry, RSC Adv. 4 (35) (2014) 18065–18073.
- [86] Y. Zhang, Y. Wang, Y. Guan, L. Feng, Uncovering the pKa dependent fluorescence quenching of carbon dots induced by chlorophenols, Nanoscale 7 (2015) 6348–6355.
- [87] F.A. Permatasari, A.H. Aimon, F. Iskandar, T. Ogi, K. Okuyama, Role of C–N configurations in the photoluminescence of graphene quantum dots synthesized by a hydrothermal route, Sci. Rep. 6 (2016) 21042.
- [88] W. Lu, X. Gong, M. Nan, Y. Liu, S. Shuang, C. Dong, Comparative study for N and S doped carbon dots: synthesis, characterization and applications for Fe³⁺ probe and cellular imaging, Anal. Chim. Acta 898 (2015) 116–127.
- [89] K. Artyushkova, B. Kiefer, B. Halevi, A. Knop-Gericke, R. Schlogl, P. Atanassov, Density functional theory calculations of XPS binding energy shift for nitrogen-containing graphene-like structures, Chem. Commun. 49 (25) (2013) 2539–2541.
- [90] D. Pan, J. Zhang, Z. Li, M. Wu, Hydrothermal route for cutting graphene sheets into blue-luminescent graphene quantum dots, Adv. Mater. 22 (6) (2010) 734–738.
- [91] Y. Tan, S. Jin, R.J. Hamers, Photostability of CdSe quantum dots functionalized with aromatic dithiocarbamate ligands, ACS Appl. Mater. Interfaces 5 (24) (2013) 12975–12983.
- [92] H. Peng, J. Travas-Sejdic, Simple aqueous solution route to luminescent carbonogenic dots from carbohydrates, Chem. Mater. 21 (2009) 5563–5565.
- [93] W. Wang, C. Damm, J. Waite, T.J. Nacken, W. Peukert, Photobleaching and stabilization of carbon nanodots produced by solvothermal synthesis, Phys.

- Chem. Chem. Phys. 18 (2016) 466–475.
- [94] X. Zhang, H. Wang, H. Wang, Q. Zhang, J. Xie, Y. Tian, J. Wang, Y. Xie, Single-layered Graphitic-C₃N₄ quantum dots for two-photon fluorescence imaging of cellular nucleus, *Adv. Mater.* 26 (2014) 4438–4443.
- [95] Q.-L. Zhao, Z.-L. Zhang, B.-H. Huang, J. Peng, M. Zhang, D.-W. Pang, Facile preparation of low cytotoxicity fluorescent carbon nanocrystals by electro-oxidation of graphite, *Chem. Commun.* (2008) 5116–5118.
- [96] S. Zhu, Q. Meng, L. Wang, J. Zhang, Y. Song, H. Jin, K. Zhang, H. Sun, H. Wang, B. Yang, Highly photoluminescent carbon dots for multicolor patterning, sensors, and bioimaging, *Angew. Chem.* 125 (2013) 4045–4049.
- [97] J.M. Janda, *The Prokaryotes: Volume 6: Proteobacteria: Gamma Subclass*, 2006.
- [98] M.H. Serres, M. Riley, Genomic analysis of carbon source metabolism of *Shewanella oneidensis* MR-1: predictions versus experiments, *J. Bacteriol.* 188 (13) (2006) 4601–4609.